Modeling and fault diagnosis of flat inland navigation canals

P. Segovia, J. Blesa, K. Horváth, L. Rajaoarisoa, F. Nejjari, V. Puig, E. Duviella

Modeling and Fault Diagnosis of Flat Inland Navigation Canals

Journal Title
XX(X):1–9

DOI: 10.1177/ToBeAssigned
www.sagepub.com/
SAGE

P. Segovia[1,2,3], J. Blesa[2,3], K. Horváth[4], L. Rajaoarisoa[1], F. Nejjari[2], V. Puig[2,3] and E. Duviella[1]

Abstract

This paper regards the development of an analytical redundancy-based approach for detecting and isolating both sensor and actuator faults in flat inland navigation canals. Inland navigation networks are principally used for transport and are composed of many canalized natural rivers and artificial canals characterized by no slope. These canals are strongly affected by resonance phenomena, which can create waves such that the navigation condition might not be guaranteed. It is therefore required to ensure dealing with fault-free measured data and actuators. The proposed approach is based on the Integrator Delay Zero (IDZ) model of the flat inland navigation canal. The proposed method is tested by considering the Cuinchy-Fontinettes navigation reach (in the north of France) to detect and isolate the occurrence of faults in the Cuinchy and Fontinettes level sensors and in the Cuinchy gate.

Keywords

Large-scale systems, open-flow water networks, modeling, fault detection and isolation

1 Introduction

Inland navigation systems extend over more than 37,000 km in Europe. An intensification of their use for transport purposes is expected in the not-too-distant future; indeed, this transport mode offers economical and environmental benefits over road transport [1]. In addition, this increase in the demand of inland waterways transport will take place in a context of climate change, which will naturally constrain its management; in particular, the water resources allocated to navigation.

Inland navigation networks can be considered as large-scale systems composed of natural canalized rivers and artificial canals, equipped with locks that make possible to navigate along them. However, their operation creates waves that not only disturb the water levels but also travel back and forth along the water stream (resonance phenomena), only attenuating after several hours. This behavior is especially critical for those reaches that are characterized by no bottom slope (*flat* reaches).

These networks are usually modeled using a decomposition in several reaches to facilitate the modeling task. A natural way to partition these systems is to consider portions of the water stream between two locks or gates, which are called navigation reaches. Their management aims at maintaining the water level around a setpoint known as the Normal Navigation Level (NNL). The allowed fluctuation of the water level is defined by means of the Higher Navigation Level (HNL) and the Lower Navigation Level (LNL). When the measured water level crosses one of these boundaries in any reach, the navigation of vessels must stop. Figure 1 illustrates this situation.

In addition, any error provided by a failure in a level sensor or a gate can lead to inefficient water and navigation control. Therefore, sensor and actuator fault diagnosis represents an important issue for inland navigation systems monitoring and supervision. This topic has attracted considerable attention in the past years, and an extense body of literature dedicated to fault diagnosis of water systems has been produced. For instance, an H_∞ observer was designed for time-varying systems, which generated residuals sensitive to some faults and insensitive to others, aiming at isolating faults on the regulation gates of a canal [2]. A fault diagnosis architecture

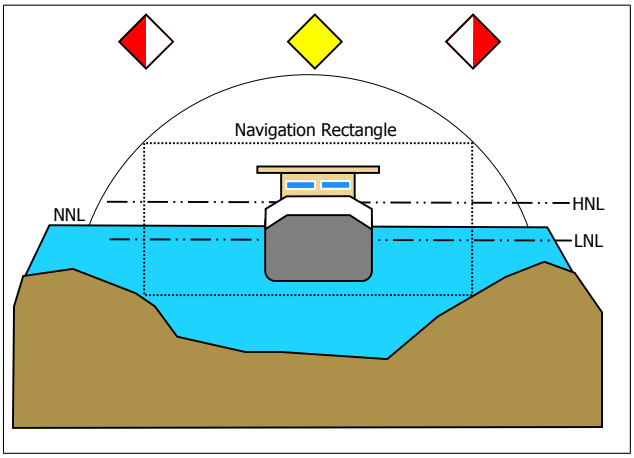

Figure 1. NNL and navigation rectangle.

[1]URIA, IMT Lille Douai, Lille, France
[2]Automatic Control Department, Technical University of Catalonia (UPC), Terrassa, Spain
[3]Institut de Robòtica i Informàtica Industrial (CSIC-UPC), Barcelona, Spain
[4]Department of Mechanical Engineering, Eindhoven University of Technology, Eindhoven, The Netherlands

Corresponding author:
P. Segovia
Email: pablo.segovia@imt-lille-douai.fr

was proposed to distinguish offtake, water level sensor and gate faults in irrigation canals[3]. A reconfigurable distributed LQG controller was designed to ensure the navigability of the canals in the presence of both sensor and actuator faults[4]. A fuzzy residual diagnosis strategy based on analytical redundancy was developed to detect and isolate faults on sensors in an urban water supply network[5]. A mathematical framework suitable for fault diagnosis and security in water systems was derived while dealing with the sensor placement problem in large-scale drinking water distribution networks[6].

In this work, a model-based passive robust fault diagnosis method is proposed, aiming at detecting and isolating possible sensor and actuator fault that can occur in inland waterways. The model is based on the Saint-Venant partial differential equations[7], which can accurately represent the dynamics of a navigation reach. However, these nonlinear differential equations cannot be solved analytically, being only possible a numerical solution, they are extremely sensitive to errors in the physical parameters and not well suited for control purposes[8]. All these reasons have fostered the development of simplified models, which are obtained by linearizing this set of equations around a certain operating point. One of the first attempts at finding a suitable simplified model was the Integrator Delay (ID) model[9], which was later improved by considering an additional zero in the model, leading to the Integrator Delay Zero (IDZ) model[10]. More recently, the Integrator Resonance (IR) model[11] was conceived for free-surface water systems whose dynamics are characterized by the resonance phenomena. In addition, grey-box[12–14] and black-box[15] models have also been proposed to deal with navigation reaches for which the physical parameters are not well known.

The present work uses the IDZ model. Many examples can be found in the literature that make use of it for fault diagnosis purposes; it is indeed an important issue for inland navigation systems because an error provided by a sensor could lead to navigation disruption[16]. For instance, it was used to detect and isolate sensor faults in combination with a pattern recognition method[17]: the IDZ model (nominal model) and the interval outputs (coming from the interval model) were used as features for the classification algorithm. Another work sought to diagnose sensor faults in the Cuinchy-Fontinettes reach (CFr)[18] in the north of France. The same reach was also considered in order to develop a diagnosis approach for sensor and actuator faults[19].

The CFr has served in many works as the case study to illustrate the proposed approaches. Indeed, it constitutes an important reach in the inland navigation network in the north of France. First of all, its location allows to control the water dispatch among the three major water catchments in the region. In addition, this reach is equipped with the biggest lock in terms of size and dispatched water volume in a single lock operation. Due to the dimensions of this lock, the dynamics of the CFr are particularly impacted by resonance phenomena. For all these reasons, it is crucial to ensure that all the possible faults in the CFr can be detected and isolated.

The first efforts towards diagnosing sensor and actuator faults in the CFr were carried out[19]: some hints about the modeling step were given and the diagnosis approach was proposed, but it was only tested for a subset of all the possible faults that can impact the system. However, in this paper the modeling methodology is detailed and the expressions of the IDZ parameters are explicitly given by considering specific features of flat navigation reaches. Furthermore, a global fault diagnosis approach is designed to detect and isolate all the possible sensor and actuator faults that can affect the system. The case study section is devoted to verify that the proposed methodology achieves the desired performance.

The structure of this paper is as follows: the description of the system, the management objectives and the constraints on the navigation conditions are presented in Section 2. The IDZ model is described in Section 3 and the necessary parameter expressions based on physical principles are given. Certain simplifications can be carried out due to the fact that the CFr is a flat reach, hence the uniform dynamics are not present in this scenario. Section 4 is dedicated to the presentation of the fault diagnosis method. Finally, Section 5 gathers all the possible faulty scenarios and illustrates them by considering the CFr as the case study, highlighting the performance of the proposed methodology. Finally, the conclusions that stem from this work are given in Section 6.

2 Problem statement

The largest inland navigation network in France is located in the north of the country. It is composed of more than 50 navigation reaches connected through locks. Some of these navigation reaches are artificial canals, which is the case of the CFr. Figure 2 depicts part of this network.

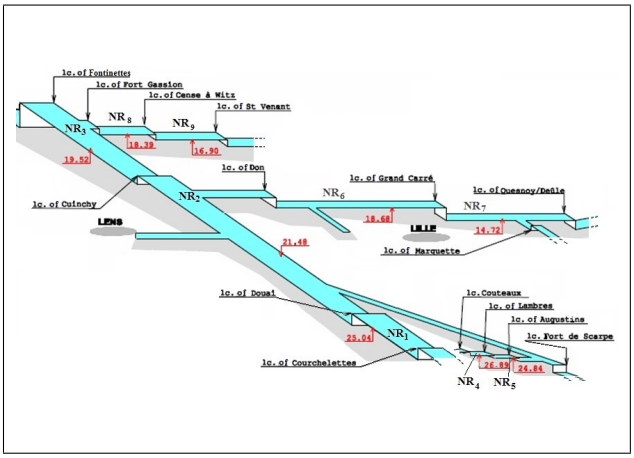

Figure 2. Schematic view of a part of the inland navigation network in the north of France.

This reach is equipped with the lock of Cuinchy at the upstream end and with the lock of Fontinettes at the downstream end. A lock operation in Cuinchy implies a water volume input of 3,700 m^3 to the CFr, while a lock operation in Fontinettes corresponds to an output volume of 25,000 m^3. As the volume outputs are significantly larger than the inputs, it is necessary to balance the water volumes that have been exchanged with the adjacent reaches during navigation periods. For this purpose, the CFr has been equipped with a controlled gate in Cuinchy, which is used to supply the CFr. The daily period of navigation corresponds to 14 hours, starting from 6 a.m. The water volume balance takes place once the navigation has stopped.

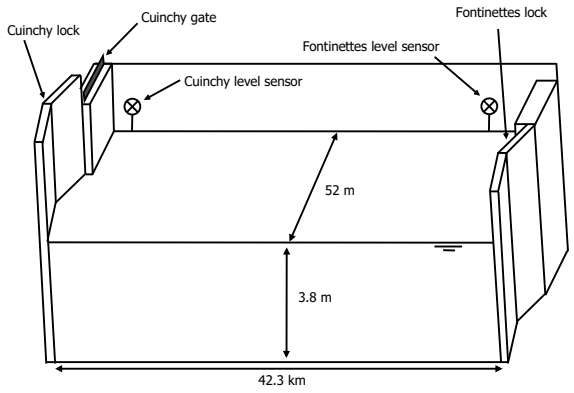

Figure 3. Schematic view of the CFr.

The CFr is characterized by no slope, a length of $42,3\ km$, a width of $52\ m$ and a variable profile geometry, which can be simplified by considering an average rectangular profile (*see* Fig. 3).

The management of the CFr consists in maintaining the water level within 3.8 (*i.e.* the NNL) $\pm$ $0.05\ m$. These boundaries correspond to the navigation rectangle. If the water level crosses the navigation rectangle, the navigation has to stop. These strong constraints on the water levels require the implementation of efficient control algorithms and fault diagnosis methodologies.

A fault diagnosis method is therefore designed in order to detect and isolate faults that can occur on the Cuinchy and Fontinettes level sensors and on the Cuinchy gate. This approach is based on the IDZ model of the CFr. The steps involved in the estimation of the IDZ parameters for flat, free-surface reaches is presented next.

3 Modeling of flat navigation canals

Many linearized models that can be used to describe the dynamics of water networks have been mentioned in the introduction. These models link the measured water depths and the discharges at the boundaries of a reach. In general, the following relationship can be considered:

$$\begin{bmatrix} y(0,s) \\ y(L,s) \end{bmatrix} = \underbrace{\begin{bmatrix} p_{11}(s) & p_{12}(s) \\ p_{21}(s) & p_{22}(s) \end{bmatrix}}_{\boldsymbol{P}(s)} \begin{bmatrix} q(0,s) \\ q(L,s) \end{bmatrix}, \tag{1}$$

where 0 and L are the abscissas for the initial and final ends of the canal; $y(0,s)$ and $y(L,s)$, the upstream and downstream water levels; $q(0,s)$ and $q(L,s)$, the upstream inflow and downstream outflow; and $p_{ij}(s)$, the different terms of the linearized model.

Among all these possibilities, in this work the IDZ model is used because of its simplicity and its capability to characterize the dynamics of the reaches with high accuracy in all regimes. It consists of an integrator, a delay and a zero: while the two first terms reproduce the low frequencies behavior, the zero accounts for the high frequencies. Its structure is as follows:

$$p_{ij}(s) = \frac{z_{ij}s + 1}{\mathcal{A}_{ij}s} e^{-\tau_{ij}s}, \tag{2}$$

where z represents the inverse of the zero, $\mathcal{A}$ the integrator gain and τ the propagation time delay. It is not possible to obtain the exact values of these parameters; however, they can be precisely approximated [10]. Since the used parameters are an estimation of the theoretical ones, the notation $\hat{p}_{ij}$ replaces p_{ij} hereinafter. The integrator gain accounts for the volume change according to the variation of the water level. The time delay represents the required time for a wave to travel from its origin to the measurement points (therefore $\tau_{11} = \tau_{22} = 0$). Finally, the zero approximates through a constant gain the oscillatory phenomena that occurs in high frequencies.

In general, these parameters are computed for both the upstream uniform and the downstream backwater part of the canal, and they are then merged into the so-called equivalent parameters, which describe the whole pool. Nevertheless, in the considered case study, the bed slope is 0 (flat canal), which means that there is no uniform flow [20]. Therefore, the parameters must only be computed for the backwater part (using the total length of the reach), and no merging formulas are needed afterward. Furthermore, as the canal presents null bottom slope, some parameters are not needed, and the general expressions of some other parameters can be simplified.

The formulas that are used to compute the parameters of the model (1) in the case of a flat canal are given below:

$$\tau_{12} = \frac{L}{C_0 + V_0} \tag{3a}$$

$$\tau_{21} = \frac{L}{C_0 - V_0} \tag{3b}$$

$$z_{11} = \frac{1}{T_0 C_0 (1 - F_0)} \sqrt{\frac{1 + \left(\frac{1-F_0}{1+F_0}\right)^2 e^{\alpha L}}{1 + e^{\alpha L}}} \tag{3c}$$

$$z_{12} = \frac{2}{T_0 C_0 (1 - {F_0}^2)} \frac{e^{-\frac{L\gamma_0}{2T_0({C_0}^2 - {V_0}^2)}}}{\sqrt{1 + e^{\alpha L}}} \tag{3d}$$

$$z_{21} = \frac{2}{T_0 C_0 (1 - {F_0}^2)} \frac{e^{\frac{L\gamma_0}{2T_0({C_0}^2 - {V_0}^2)}}}{\sqrt{1 + e^{\alpha L}}} \tag{3e}$$

$$z_{22} = \frac{1}{T_0 C_0 (1 + F_0)} \sqrt{\frac{1 + \left(\frac{1+F_0}{1-F_0}\right)^2 e^{\alpha L}}{1 + e^{\alpha L}}} \tag{3f}$$

$$A_{11} = A_{12} = \frac{{T_0}^2 \left({C_0}^2 - {V_0}^2\right)}{\gamma_0} \left(e^{\frac{\gamma_0 L}{T_0({C_0}^2 - {V_0}^2)}} - 1 \right) \tag{3g}$$

$$A_{21} = A_{22} = \frac{{T_0}^2 \left({C_0}^2 - {V_0}^2\right)}{\gamma_0} \left(1 - e^{-\frac{\gamma_0 L}{T_0({C_0}^2 - {V_0}^2)}} \right) \tag{3h}$$

with L $[m]$ the length of the reach, C_0 $[m/s]$ the water celerity, V_0 $[m/s]$ the average water velocity, T_0 $[m]$ the top width, F_0 (dimensionless) the Froude number, α $[m^{-1}]$ and γ_0 $[m^2 s^{-2}]$ two geometrical coefficients. Some of these parameters must be evaluated in a precise spatial abscissa of the reach; in this case, the value $x = L/2$ is used, except where otherwise noted.

In order to compute the parameters (3a)–(3h), the following expressions must be used:

$$C_0 = \sqrt{\frac{gA_0}{T_0}} \tag{4a}$$

$$V_0 = \frac{Q_0}{A_0} \tag{4b}$$

$$F_0 = \frac{V_0}{C_0} \tag{4c}$$

$$\alpha = -\frac{T_0}{A_0 F_0 \left(1 - {F_0}^2\right)} \left[2 + (K_0 - 1){F_0}^2 - \left(\frac{A_0}{{T_0}^2} \frac{dT_0}{dY} + \kappa_0 - 2 \right) {F_0}^4 \right] \tag{4d}$$

$$\gamma_0 = {V_0}^2 \frac{\partial T_0}{\partial x} - gT_0 \left[1 + \kappa_0 - (\kappa_0 - 2){F_0}^2 \right] \frac{\partial Y_0}{\partial x} \tag{4e}$$

$$\kappa_0 = \frac{7}{3} - \frac{4A_0}{3T_0 P_0} \frac{\partial P_0}{\partial Y} \tag{4f}$$

$$\frac{\partial Y_0}{\partial x} = \frac{-s_{f0}(x)}{1 - {F_0}^2(x)} \tag{4g}$$

$$s_{f0}(x) = \frac{{Q_0}^2 n^2}{{A_0}^2(x) {R_0}^{4/3}(x)} \tag{4h}$$

$$R_0 = \frac{A_0}{P_0} \tag{4i}$$

with g $[ms^{-2}]$ the gravitational acceleration, A_0 $[m^2]$ the wetted area, κ_0 and s_L (dimensionless) two geometrical coefficients linked to the shape of the reach, Y_0 $[m]$ the water depth, x $[m]$ the position along the reach, s_{f0} (dimensionless) the friction slope, Q_0 $[m^3 s^{-1}]$ the reference discharge across section A_0, n $[sm^{-1/3}]$ the roughness coefficient, R_0 $[m]$ the hydraulic radius and P_0 $[m]$ the wetted perimeter. The derivatives $\frac{dT_0}{dY}$, $\frac{\partial T_0}{\partial x}$, $\frac{\partial Y_0}{\partial x}$ and $\frac{\partial P_0}{\partial Y}$ can be computed according to the geometry of the reach.

The following transfer functions are obtained when the expressions (3a)–(3h) and (4a)–(4i) are used:

$$\hat{p}_{11} = \frac{6928s + 1}{2.2 \cdot 10^6 s} \tag{5a}$$

$$\hat{p}_{12} = \frac{-9544s - 1}{2.2 \cdot 10^6 s} e^{-6930s} \tag{5b}$$

$$\hat{p}_{21} = \frac{9544s + 1}{2.2 \cdot 10^6 s} e^{-6920s} \tag{5c}$$

$$\hat{p}_{22} = \frac{-6928s - 1}{2.2 \cdot 10^6 s} \tag{5d}$$

A reference discharge $Q_0 = 0.6 m^3/s$ and a roughness coefficient $n = 0.035$ have been considered in the present case.

The performance of this model is compared with the results obtained using the hydraulic simulator SIC^2 (http://sic.g-eau.net), developed at IRSTEA Montpellier[21]. SIC^2 solves numerically the Saint-Venant equations without simplification. Hence, the results provided by this software will be taken as the reference to check the predictive power of the computed IDZ model. The predictive power of the IDZ model has already been tested and validated in different realistic scenarios for the CFr[22].

It will be seen later how the IDZ model predicts the correct downstream water level, but it is not the case for the upstream water level. This mismatch in the estimation of the upstream water level is corrected by means of the following calibration strategy:

$$\hat{p}'_{ij}(s) = \frac{k_{ij} \cdot z_{ij} s + 1}{\mathcal{A}_{ij} s} e^{-\tau_{ij} s}, \tag{6}$$

where k_{ij} are the calibration coefficients. Notice that only the zeros are calibrated: indeed, the mismatch between the reference and the IDZ model mainly affects the peak response, for which the zero accounts. Therefore, this calibration aims at reproducing the peak magnitude with more accuracy.

The models are calibrated for the Fontinettes lock operation, as it involves the largest water volume dispatch. The calibrated IDZ model for the upstream water level is:

$$\hat{p}'_{11}(s) = \frac{5995s + 1}{2.2 \cdot 10^6 s} \tag{7a}$$

$$\hat{p}'_{12}(s) = \frac{-7003s - 1}{2.2 \cdot 10^6 s} e^{-6930s} \tag{7b}$$

Since the downstream water level was correctly predicted from the beginning, no calibration is needed for the first two terms. Therefore, $\hat{p}'_{21}(s) = \hat{p}_{21}(s)$ and $\hat{p}'_{22}(s) = \hat{p}_{22}(s)$.

Figure 4 shows the evolution of the water level at the upstream and downstream ends for the reference, the original *uncalibrated* IDZ model (5) and the calibrated IDZ model (7). Notice that only the first peak in the response is shown. Indeed, a lock operation is simulated in Fontinettes at $t = 0.5$ h, whose effect can be observed in Cuinchy after τ_d (at $t \approx 2.5$ h), which is the time required for a perturbation to travel from the downstream to the upstream end. It is shown that the calibrated model provides a more accurate prediction of the upstream water level.

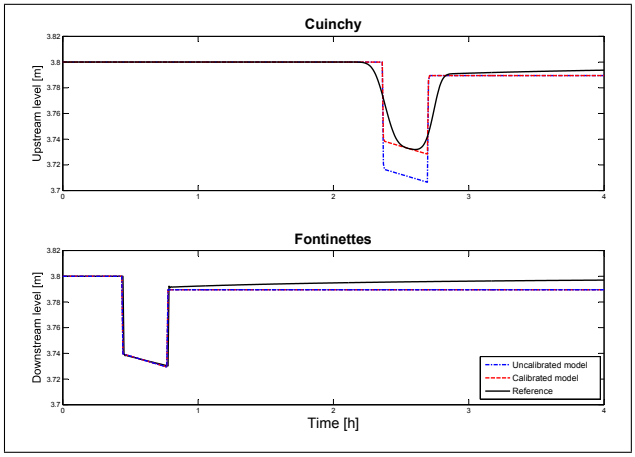

Figure 4. Evolution of the water levels for the Fontinettes lock operation.

4 Fault diagnosis

A fault diagnosis method for the CFr based on the flat navigation canals model presented in Section 3 is proposed. Fault diagnosis is usually divided in two parts: fault detection and fault isolation.

4.1 Fault detection

Model-based fault detection is built on checking the consistency between the measured inputs and outputs from a system and the behavior described by a model of the faultless system. The presence of a fault is proved when the model of the faultless system is not consistent with the available measurements. The model of the system should describe the behavior of the system in any non-faulty scenario and also in faulty scenarios where the fault can be modeled by a change of model parameters or variables.

In the case of the use of qualitative models, *i.e.* mathematical models that can be described in time or frequency domain, the fault diagnosis is usually based on the evaluation of a temporal residual $r(t)$ [23–25]. Also known as analytical redundancy, a temporal residual is computed as the difference between the real observed behavior of a system $y(t)$ provided by sensors and the predicted $\hat{y}(t)$ by the model, *i.e.*

$$r(t) = y(t) - \hat{y}(t) \tag{8}$$

In an ideal case, residuals should only be different from zero when the system is affected by a fault. However, due to modeling errors, sensor noises and disturbances, the residuals can be different from zero in non-faulty scenarios. Therefore, residual-based fault detection methods must consider this fact (should be robust) in order to avoid false alarms.

A passive robust fault detection method can be implemented by means of the computation of the maximum positive and negative deviations (bounds $\overline{\sigma}$ and $\underline{\sigma}$) of the residual $r(t)$ in the time domain from zero in a non-faulty scenario. Therefore, the values of the bounds are directly linked to the accuracy of the model. The fault detection test can be formulated as:

$$\phi(t) = \begin{cases} 0 \text{ if } r(t) \in [\underline{\sigma}, \overline{\sigma}] \Rightarrow \text{ No Fault} \\ 1 \text{ otherwise} \end{cases} \tag{9}$$

The main drawback of the fault detection test defined by (9) is that some faults whose effect in the residual is not large enough to reach the threshold are not detected (undetected faults). This means that a minimum fault magnitude is necessary to guarantee its detection. This minimum detectable fault guarantees that the residual reaches its threshold (*triggering limit*)[23] despite of model uncertainties.

4.2 Fault isolation

Fault isolation usually requires the evaluation of a set of residuals $r_1, \ldots, r_{n_r}$ that derives a set of fault signals $\phi_1, \ldots, \phi_{n_r}$ computed, for instance, by means of (9). In this paper, the fault isolation strategy that will be used is based on previous works [26,27] (*see* Fig. 5).

First, a memory component updates cyclically the fault signal occurrence provided by the fault detection algorithm. When a fault is detected, the information of the different fault signals are stored in a table. This information consists of the first fault signal activation time t_o, the activation time of the other signals t_i that are activated in the time window $t \in [t_o, t_o + T_w]$ (where T_w is a prefixed waiting time) and the maximum activation value $\phi_{i,\max}$ for every fault signal

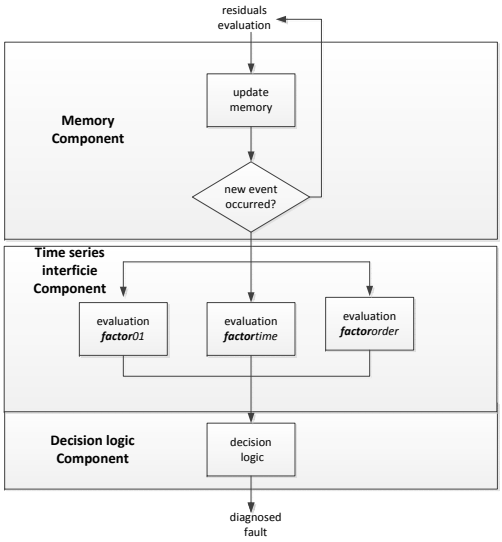

Figure 5. Fault isolation components.

ϕ_i $i = 1, ..., n_r$ in this time window computed as:

$$\phi_{i,\max}(t) = \max_{l \in [t_o, t]} |\phi_i(l)| \tag{10}$$

with $t \leq t_o + T_W$ where T_w must be chosen as the largest transient time response T_{lt} from a fault-free scenario to any faulty scenario. The advantage of using maximum activation values $\phi_{i,\max}(t)$ computed by (10) instead of temporal fault signals $\phi_i(t)$ is that the undesirable effect of non-persistent fault indicators, sensor noises and disturbances is minimized.

Once a new event has been detected in the memory component, different time series analysis are carried out to compare the observed fault behavior with the different considered fault patterns. In the fault isolation module described in Fig. 5, three different analysis are considered. One is the standard static Boolean analysis (denoted as ***factor***$01(t)$), where a Boolean fault signal activation matrix (**FSM**01) that contains information about the incidence or no incidence of faults (columns) on residuals (rows) is used to determine which is the most probable fault. The probability of a fault is determined by the match between the columns of the **FSM**01 matrix and a vector whose components are $\phi_{i,\max}$ $i = 1, ..., n_r$. ***factor***01_j is calculated for all the fault hypotheses $j = 1, ..n_f$ in the following way:

$$\textbf{\textit{factor}}01_j(t) = \frac{\sum_{i=1}^{n_r} (\phi_{i,\max}(t)\textbf{FSM}01_{ij})}{\sum_{i=1}^{n_r} \textbf{FSM}01_{ij}} \textbf{\textit{zvf}}_j(t) \tag{11}$$

where $\boldsymbol{zvf}_j$ is a zero-violation-factor defined as

$$\textbf{\textit{zvf}}_j(t) = \begin{cases} 0 \quad \text{if } \exists \mathrm{i} \in \{1, ..., \mathrm{n_r}\}, \text{with } \textbf{FSM}01_{ij} = 0 \\ \qquad\qquad\qquad\qquad \text{and } \phi_{\mathrm{i,max}}(\mathrm{t}) = 1 \\ 1 \quad \text{otherwise} \end{cases} \tag{12}$$

The fault signal occurrence order analysis (denoted as ***factor***order) compares the order of activation of the different fault signals with the expected order for all the considered

faults stored in the matrix (**FSM**order). ***factor***$order_j$ is calculated for all the fault hypotheses $j = 1, ..n_f$ in the following way:

$$\begin{aligned} &\textbf{\textit{factor}}order_j(t) = \\ &= \frac{\sum_{i=1}^{n_r} \left(order\left(\phi_{i,\max}(t), \textbf{FSM}order_{ij}\right)\right)}{\sum_{i=1}^{n_r} boolean(\textbf{FSM}order_{ij})} \cdot \textbf{\textit{zvf}}order_j(t) \end{aligned} \tag{13}$$

where

$$\begin{aligned} &order(\phi_{i,\max}(t), \textbf{FSM}order_{ij}) = \\ &= \begin{cases} 0, & order(\phi_{i,\max}(t)) \neq \textbf{FSM}order_{ij} \\ 1, & order(\phi_{i,\max}(t)) = \textbf{FSM}order_{ij} \end{cases} \end{aligned} \tag{14}$$

and ***zvf***$order_j(t)$ is defined as ***zvf***$_j(t)$ in (12) but excluding those fault hypotheses that do not coincide in the order.

The time occurrence analysis (denoted as ***factor***time) checks the consistency of the delay between the different fault activation signals and the time of the first fault signal activation time t_o and the expected one stored in the matrix (*FSM*time), whose components are computed as

$$\textbf{FSM}time_{ij} = \begin{cases} [\underline{\tau}_{ij}, \overline{\tau}_{ij}] & if \quad \textbf{FSM}_{ij} = 1 \\ [-1, -1] & if \quad \textbf{FSM}_{ij} = 0 \end{cases} \tag{15}$$

where $[\underline{\tau}_{ij}, \overline{\tau}_{ij}]$ is the time interval in which the fault signal ϕ_i caused by fault f_j is expected to appear. ***factor***$time_j$ is calculated for all the fault hypotheses $j = 1, ..n_f$ in the following way:

$$\begin{aligned} &\textbf{\textit{factor}}time_j(t) = \\ &= \frac{\sum_{i=1}^{nr} \left(checktime\left(t_{\phi i}, t_{ref}, \textbf{FSM}time_{ij}\right)\right)}{\sum_{i=1}^{nr} boolean(\textbf{FSM}time_{ij})} \cdot \textbf{\textit{zvf}}order_j(t) \end{aligned} \tag{16}$$

where t_{ϕ_i} is the apparition time instant of the fault signal $\phi_i(t)$, t_{ref} is the apparition time instant of the first observed fault signal

$$\begin{aligned} &checktime\left(t_{\phi i}, t_{ref}, \textbf{FSM}time_{ij}\right) = \\ &= \begin{cases} 0 & if\ t_{\phi i} - t_{ref} \notin \textbf{FSM}time_{ij} \\ 1 & if\ t_{\phi i} - t_{ref} \in \textbf{FSM}time_{ij} \end{cases} \end{aligned} \tag{17}$$

$$boolean(\textbf{FSM}time_{ij}) = \begin{cases} 0 & \text{if } \textbf{FSM}time_{ij} = [-1, -1] \\ 1 & \text{if } \textbf{FSM}time_{ij} \neq [-1, -1] \end{cases} \tag{18}$$

Finally, the most probable fault among all the possible candidates is selected by means of a decision logic block, considering the result of the different time-series analysis. A ***factor***$total_j$ is calculated for all the fault hypotheses $j = 1, ..n_f$ in the following way:

$$\begin{aligned} \textbf{\textit{factor}}total_j(t) = \textbf{\textit{factor}}01_j(t) + \textbf{\textit{factor}}order_j(t) + \\ + \textbf{\textit{factor}}time_j(t) \end{aligned} \tag{19}$$

Then, the most probable fault can be computed as

$$\hat{f}(t) = \underset{\forall j=1,\ldots,n_f}{\arg\max}\ \textbf{\textit{factor}}total_j(t) \tag{20}$$

The isolation decision must be made in a time not greater than the waiting time T_w, i.e. $t \leq t_o + T_W$, which can be computed as

$$T_w = \max_{\forall i,j}(\overline{\tau}_{ij}) \tag{21}$$

During this period of time, a likelihood index $P_j(t)$ for every fault hypothesis $j = 1, ..n_f$ can be computed as

$$P_j(t) = \frac{\textbf{\textit{factor}}total_j(t)}{\sum_{i=1}^{n_f} \textbf{\textit{factor}}total_i(t)} \tag{22}$$

4.3 Fault diagnosis in the CFr system

Two different residuals $r_C(t)$ and $r_F(t)$ can be generated for the CFr from the difference between the available level measurements in Cuinchy and Fontinettes ($y_C(t)$ and $y_F(t)$) and the level estimations ($\hat{y}_C(t)$ and $\hat{y}_F(t)$). They can be computed using (1) with:

$$\hat{y}_C(t) = \mathscr{L}^{-1}\{y(0,s)\} \text{ and } \hat{y}_F(t) = \mathscr{L}^{-1}\{y(L,s)\} \tag{23}$$

and considering that

$$q(0,s) = \mathscr{L}\{q_C(t)\} \text{ and } q(L,s) = \mathscr{L}\{q_F(t)\}, \tag{24}$$

where $\mathscr{L}\{\}$ is the Laplace transform, and $q_C(t)$ and $q_F(t)$ are the total flows in Cuinchy and Fontinettes, respectively. These flows are computed as the sum of the flows through the hydraulic equipment (gates and locks). In the case of Cuinchy, there is a lock with a known operation profile $q_{lock_C}(t)$ and a controlled gate with the known input $u_C(t)$. On the other hand, there is only a lock with a known operation profile $q_{lock_F}(t)$ in Fontinettes.

The possible faults that can impact the CFr are sensor faults in both level sensors f_{y_C} and f_{y_F} and actuator faults in the Cuinchy control gate f_{u_C}. The effects of the considered faults in the different variables involved in the two residual computations are:

$$\begin{aligned} y_C(t) &= y_C^0(t) + f_{y_C}(t) \\ y_F(t) &= y_F^0(t) + f_{y_F}(t) \\ q_C(t) &= q_{lock_C}(t) + u_C(t) = q_{lock_C}(t) + u_C^0(t) + f_{u_C}(t) \\ q_F(t) &= q_{lock_F}(t) \end{aligned}$$

where $y_C^0(t)$, $y_F^0(t)$ and $u_C^0(t)$ denote actual values of levels and control gate flow, respectively.

Then, considering the effect of the three faults in the two residuals, matrices **FSM**01 (Table 1), **FSM**order (Table 2) and **FSM**time (Table 3) can be obtained. The level sensor faults f_{y_C} and f_{y_F} only affect the associated level residual. Thus, the **FSM**order matrix does not provide any additional information to the **FSM**01 matrix and neither does the **FSM**time matrix, where [-1,-1] denotes no influence of a fault in a residual[27]. On the other hand, f_{u_C} affects the two level residuals, first r_C and later r_F. The time values $\underline{\tau}_{2,3}$ and $\overline{\tau}_{2,3}$ denote the minimum and maximum delays from the

activation of the fault signal in r_C to the activation of r_F in the presence of an actuator fault in the Cuinchy control gate f_{u_C}. Therefore, when the fault signal associated to the Cuinchy level residual is activated, a waiting time $T_w = \overline{\tau}_{2,3}$ has to be considered in (10) to distinguish between a fault in the Cuinchy level sensor (f_{y_C}) and an actuator fault in the Cuinchy control gate (f_{u_C}). The values of $\underline{\tau}_{2,3}$ and $\overline{\tau}_{2,3}$ will be around the delay of the transfer function $\hat{p}'_{12}(s)$ (*i.e.* 6930 s).

	f_{y_C}	f_{y_F}	f_{u_C}
r_C	1	0	1
r_F	0	1	1

Table 1. **FSM**01 matrix in the CFr system

	f_{y_C}	f_{y_F}	f_{u_C}
r_C	1	0	1
r_F	0	1	2

Table 2. **FSM**order matrix in the CFr system

	f_{y_C}	f_{y_F}	f_{Q_C}
r_C	0	[-1,-1]	0
r_F	[-1,-1]	0	$[\underline{\tau}_{2,3}, \overline{\tau}_{2,3}]$

Table 3. **FSM**time matrix in the CFr system

5 Results

The IDZ models obtained in (7) are used to compute the results. On the other hand, in order to cope with errors due to uncertainty in transport delays that are present in open-flow canal systems, following the ideas of previous works[28], the residual has been computed as

$$r(t) = y(t) - \hat{y}(t - \Delta\tau^0), \tag{26}$$

where

$$\Delta\tau^0 = \arg \min_{\Delta\tau \in [-\lambda_\tau, \lambda_\tau]} |y(t) - \hat{y}(t - \Delta\tau)|, \tag{27}$$

with λ_τ the maximum deviation from the nominal time delay.

Uncertainties in time delays lead to important instantaneous errors in level estimations. Figure 6 shows the evolution of residuals computed directly with (8) and applying (26) in a realistic scenario. Maximum and minimum residual values in fault-free scenarios have been chosen as residual bounds $\underline{\sigma}$ and $\overline{\sigma}$ used in the fault detection procedure (9). The residual bounds for the two residuals computed directly and applying (26) by considering $\lambda_\tau = 120\ s$ in (27) are summarized in Table 4.

	Directly		Applying $\Delta\tau$	
	$\underline{\sigma}$	$\overline{\sigma}$	$\underline{\sigma}$	$\overline{\sigma}$
$r_C[m]$	-0.062	0.052	-0.05	0.042
$r_F[m]$	-0.096	0.096	-0.032	0.013

Table 4. Residual fault detection thresholds

All the realistic fault scenarios that can impact the system have been generated in order to study the performance of the proposed fault diagnosis method considering *FSM*01 (Table 1), *FSM*order (Table 2) and *FSM*time (Table 3) with $\underline{\tau}_{2,3} = 5900\ s$ and $\overline{\tau}_{2,3} = 7900\ s$.

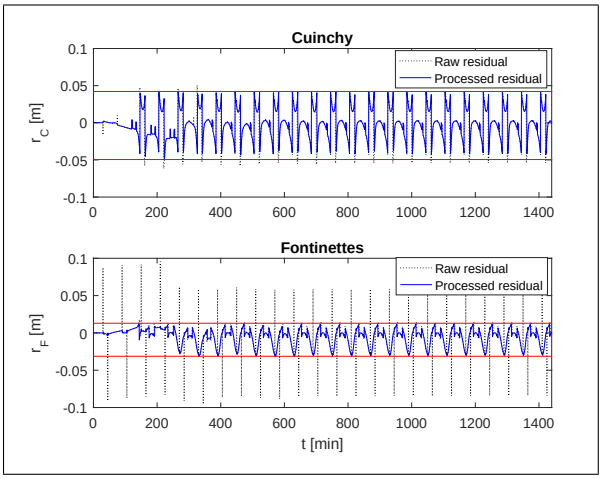

Figure 6. Level residuals $r_C(t)$ and $r_F(t)$ in a 24-hour fault-free scenario.

With the purpose of avoiding that uncertainty and modeling errors compensate the fault effects, when a fault is detected using (9), the residual is computed using (26) by considering $\Delta\tau^0$ computed with (27), but changing min by max. In the following, the results of these three faulty scenarios are explained in detail.

5.1 Level sensor fault in Cuinchy

An additive fault of 6 cm is simulated at the Cuinchy level sensor at $t \geq 250\ min$, emulating a fall of 6 cm of an ultrasonic sensor from its support arm. Figure 7 shows the evolution of the two residuals: only $r_C(t)$ is activated when the fault is produced (at $t = 250\ min$). Then, applying (19) and considering Tables 1, 2 and 3, the Fontinettes sensor fault hypothesis provides a ***factor***$total_j$ equal to zero and the Cuinchy sensor and actuator faults hypothesis provide a ***factor***$total_j$ equal to 3 and 1.5 respectively and therefore the most probable fault with a likelihood index P_j (22) equal to 6.67 is the Cuinchy sensor fault hypothesis, this hypothesis is confirmed after the waiting time $T_W = 7900s$ with no more activated signals.

5.2 Level sensor fault in Fontinettes

An additive fault of 6 cm is simulated at the Fontinettes level sensor at $t \geq 500\ min$, which emulates a fall of 6 cm of an ultrasonic sensor from its support arm. Figure 8 shows the evolution of the two residuals: $r_F(t)$ is activated when the fault is produced (at $t = 500\ min$). Then, applying (19) and considering Tables 1, 2 and 3, the only fault that provides a ***factor***$total_j$ different from zero is the Fontinettes sensor fault and therefore the fault is correctly isolated.

5.3 Actuator fault in Cuinchy

An additive fault of $-4\ m^3/s$ is simulated at the Cuinchy control gate at $t \geq 300\ min$ that emulates a partial obstruction in this gate. Figures 9 and 10 show the residuals and the fault signals evolution, respectively. The first fault signal $\phi_C(t)$ is activated at $t = 342\ min$ (42 min after the gate is partially blocked). Later, at $t = 442\ min$, the

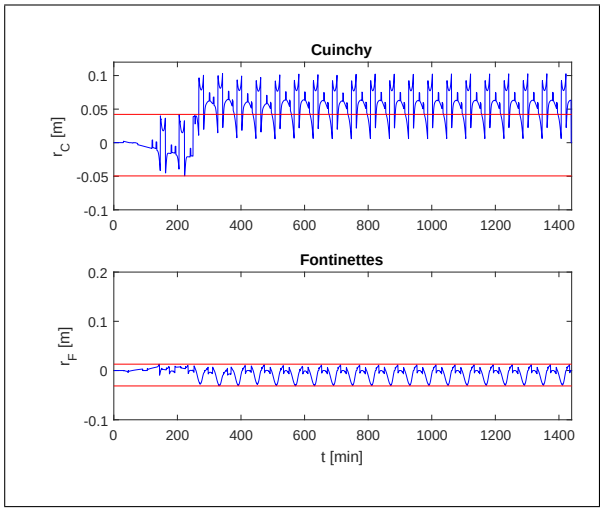

Figure 7. Water level residuals $r_C(t)$ and $r_F(t)$ in a sensor fault scenario: Cuinchy level fault $f_{y_C}(t) = 6\ cm$ at $t \geq 250\ min$

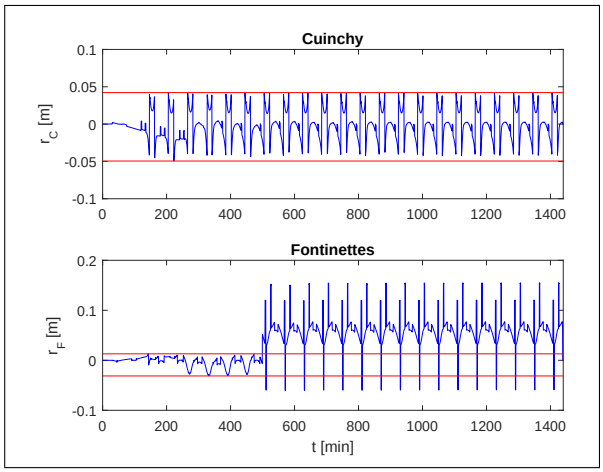

Figure 8. Water level residuals $r_C(t)$ and $r_F(t)$ in a sensor fault scenario: Fontinettes level fault $f_{y_F}(t) = 6\ cm$ at $t \geq 500\ min$.

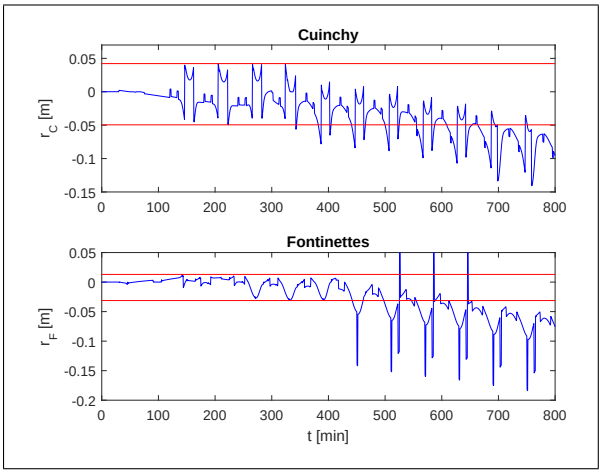

Figure 9. Level residuals $r_C(t)$ and $r_F(t)$ in an actuator fault scenario: Cuinchy fault $f_{u_C}(t) = -4\ m^3/s$ at $t \geq 300\ min$

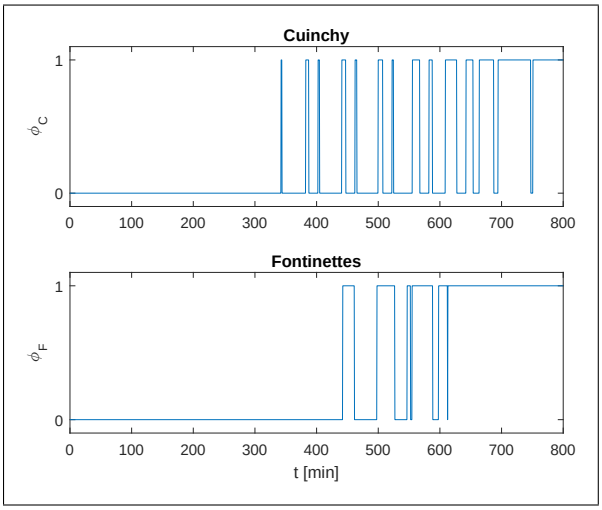

Figure 10. Instantaneous activation signals $\phi_C(t)$ and $\phi_F(t)$ in an actuator fault in Cuinchy ($f_{u_C}(t) = -4\ m^3/s$ at $t \geq 300\ min$)

fault signal $\phi_F(t)$ is activated. Then, during 100 min (from $t = 342\ min$ to $t = 442\ min$), there are two fault candidates (f_{y_C} and f_{u_C}) according to Tables 1, 2 and 3, which provide likelihood indices (22) equal to 0.67 and 0.33, respectively. However, after the activation of $\phi_F(t)$, only f_{u_C} is consistent with the observed fault signals, $\boldsymbol{factor}total_j$ different from zero. The fault diagnosis procedure works despite the signal faults are intermittently activated, thanks to the memory component (10) and Table 3.

6 Conclusions

A diagnosis method was proposed in this paper to detect and isolate sensor and actuator faults that can occur in flat navigation canals. Fault diagnosis in these systems is required to avoid the navigation disruption. Indeed, the navigation is allowed only if the level of each reach is inside a navigation rectangle defined by two boundaries around the NNL. The proposed diagnosis method was designed based on the IDZ model, which is able to reproduce the peaks introduced by the significant magnitude of the lock operations. Specifically, only flat canals like the CFr were considered, thus dealing with a particular flow profile to test the proposed modeling and fault diagnosis approaches. The considered faulty scenarios correspond to all the possible faults that can impact the system. They are based on realistic operating conditions and are built to highlight the performance of the proposed diagnosis approach.

The results show that all the faults can be correctly detected, and the faulty component can be successfully isolated in all scenarios. In the case of sensor faults, only one residual is activated, which makes the diagnosis task easier. In the case of a fault in the downstream actuator, the activation of two fault signals (at different time instants) is consistent with only one possible fault, which allows to isolate the faulty component. Notice that each of the presented scenarios considers only one fault. Indeed, the next step derived from this work will address simultaneous fault occurrences. Furthermore, this diagnosis approach must be improved to deal with the strong disturbances that characterize real environmental systems.

Acknowledgements

This work has been partially funded by the Spanish Ministry of Economy and Competitiveness (MINECOP) and FEDER through the project HARCRICS (ref. DPI2014-58104- R) and through the grant IJCI-2014-20801.

References

1. C. Brand, M. Tran, and J. Anable, "The UK transport carbon model: An integrated life cycle approach to explore low carbon futures." *Energy Policy*, vol. 41, pp. 107–124, 2012.
2. N. Bedjaoui, X. Litrico, D. Koenig, and P. Malaterre, "H_∞ observer for time-delay systems Application to FDI for irrigation canals," in *45th IEEE Conference on Decision and Control*. IEEE, 2006, pp. 532–537.
3. J. L. Nabais, L. Mendonça, and M. A. Botto, "New fault isolation architecture for irrigation canals," *IFAC Proceedings Volumes*, vol. 45, no. 20, pp. 450–455, 2012.
4. J. M. Lemos and I. Sampaio, "Reconfigurable distributed control of water delivery canals," in *10th IEEE International Conference on Networking, Sensing and Control (ICNSC)*. IEEE, 2013, pp. 451–456.
5. J. Ragot and D. Maquin, "Fault measurement detection in an urban water supply network," *Journal of Process Control*, vol. 16, no. 9, pp. 887–902, 2006.
6. D. G. Eliades and M. M. Polycarpou, "A fault diagnosis and security framework for water systems," *IEEE Transactions on Control Systems Technology*, vol. 18, no. 6, pp. 1254–1265, 2010.
7. V. T. Chow, "Open-channel hydraulics." *McGraw-Hill. New York.*, 1959.
8. Y. Bolea, V. Puig, and J. Blesa, "Linear parameter varying modeling and identification for real-time control of open-flow irrigation canals," *Environmental modelling & software*, vol. 53, pp. 87–97, 2014.
9. J. Schuurmans, A. Clemmens, S. Dijkstra, A. Hof, and R. Brouwer, "Modeling of irrigation and drainage canals for controller design," *Journal of Irrigation and Drainage Engineering, December*, vol. 125, no. 6, 1999.
10. X. Litrico and V. Fromion, "Simplified modeling of irrigation canals for controller design," *Journal of Irrigation and Drainage Engineering*, pp. 373–383, 2004.
11. P. van Overloop, I. Miltenburg, X. Bombois, A. Clemmens, R. Strand, N. van de Giesen, and R. Hut, "Identification of resonance waves in open water channels," *Control Engineering Practice, Volume 18, Issue 8, August*, pp. 863–872, 2010.
12. E. Duviella, L. Bako, M. Sayed-Mouchaweh, J. Blesa, Y. Bolea, V. Puig, and K. Chuquet, "Inland navigation channel model: Application to the Cuinchy-Fontinettes reach," in *10th IEEE International Conference on Networking, Sensing and Control (ICNSC)*. IEEE, 2013, pp. 164–169.
13. K. Horváth, E. Duviella, J. Blesa, L. Rajaoarisoa, Y. Bolea, V. Puig, and K. Chuquet, "Gray-box model of inland navigation channel: application to the Cuinchy-Fontinettes reach," *Journal of Intelligent Systems*, vol. 23, no. 2, pp. 183–199, 2014.
14. I. Mareels, E. Weyer, and S. K. Ooi, "Irrigation networks: a systems engineering approach," in *Proceedings of the 4th International Conference on Control and Automation (ICCA'03)*. IEEE, 2003, pp. 15–28.
15. E. Weyer, "System identification of an open water channel," *Control Engineering Practice*, vol. 9, no. 12, pp. 1289 – 1299, 2001.
16. P. Segovia, L. Rajaoarisoa, F. Nejjari, J. Blesa, V. Puig, and E. Duviella, "Decentralized fault-tolerant control of inland navigation networks: a challenge," *Journal of Physics: Conference Series*, vol. 783, no. 1, p. 012018, 2017.
17. K. Horváth, J. Blesa, E. Duviella, L. Rajaoarisoa, V. Puig, and K. Chuquet, "Sensor fault diagnosis of inland navigation system using physical model and pattern recognition approach," *IFAC Proceedings Volumes*, vol. 47, no. 3, pp. 5309–5314, 2014, 19th IFAC World Congress.
18. J. Blesa, K. Horváth, E. Duviella, V. Puig, Y. Bolea, L. Rajaoarisoa, and K. Chuquet, "Model-based sensor supervision in inland navigation networks: Cuinchy-Fontinettes case study," *Journal of Maritime Research*, vol. 11, no. 2, pp. 81–88, 2014.
19. P. Segovia, L. Rajaoarisoa, E. Duviella, J. Blesa, F. Nejjari, V. Puig, and K. Horváth, "Fault detection and isolation in flat navigation canals," in *2017 4th International Conference on Control, Decision and Information Technologies (CoDIT)*, April 2017, pp. 0427–0432.
20. X. Litrico and V. Fromion, *Modeling and Control of Hydrosystems*. Springer, 2009.
21. P.-O. Malaterre, D. Dorchies, and J.-P. Baume, "Automatic tuning of robust PI controllers for a cascade of rivers or irrigation canals pools," *European Control Conference, Strasbourg, France, June 24-27*, 2014.
22. P. Segovia, L. Rajaoarisoa, F. Nejjari, V. Puig, and E. Duviella, "Modeling of interconnected flat open-channel flow: application to inland navigation canals," in *SimHydro 2017 Conference*, 2017.
23. J. Gertler, *Fault Detection and Diagnosis in Engineering Systems*. New York: Marcel Dekker, 1998.
24. M. Blanke, M. Kinnaert, J. Lunze, and M. Staroswiecki, *Diagnosis and fault-tolerant control*. Springer-Verlag Berlin Heidelberg, 2006.
25. R. Isermann, *Fault Diagnosis Systems: An Introduction from Fault Detection to Fault Tolerance*. Springer, New York, 2006.
26. J. Meseguer, V. Puig, and T. Escobet, "Fault diagnosis using a timed discrete-event approach based on interval observers: Application to sewer networks," *IEEE Transactions on Systems, Man, and Cybernetics Part A:Systems and Humans*, vol. 40, no. 5, pp. 900–916, 2010.
27. V. Puig and J. Blesa, "Limnimeter and rain gauge FDI in sewer networks using an interval parity equations based detection approach and an enhanced isolation scheme," *Control Engineering Practice*, vol. 21, no. 2, pp. 146–170, 2013.
28. J. Blesa, V. Puig, and Y. Bolea, "Fault detection using interval LPV models in an open-flow canal," *Control Engineering Practice*, vol. 18, no. 5, pp. 460–470, 2010.